FERMILAB-PUB-94-452-A

Nevis R#1502

Determination of the Strange Quark Content of the Nucleon from a Next-to-Leading-Order QCD Analysis of Neutrino Charm Production

A.O. Bazarko, C.G. Arroyo, K.T. Bachmann,[a] T. Bolton, C. Foudas,[b] B.J. King,[c]
W.C. Lefmann, W.C. Leung, S.R. Mishra,[d] E. Oltman,[e] P.Z. Quintas,[f]
S.A. Rabinowitz, F.J. Sciulli, W.G. Seligman, M.H. Shaevitz
Columbia University, New York, NY 10027
F.S. Merritt, M.J. Oreglia, B.A. Schumm,[e]
University of Chicago, Chicago, IL 60637
R.H. Bernstein, F. Borcherding, H.E. Fisk, M.J. Lamm,
W. Marsh, K.W.B. Merritt, H.M. Schellman,[g] D.D. Yovanovitch
Fermilab, Batavia, IL 60510
A. Bodek, H.S. Budd, P. de Barbaro, W.K. Sakumoto
University of Rochester, Rochester, NY 14627
T. Kinnel, P.H. Sandler,[h] W.H. Smith
University of Wisconsin, Madison, WI 53706.

(CCFR Collaboration)

December 9, 2013.
Submitted to Physics Letters B.

[a]Present address: National Center for Atmospheric Research, Boulder, CO 80307.
[b]Present address: University of Wisconsin, Madison, WI 53706.
[c]Present address: CERN, CH-1211 Geneva 23, Switzerland.
[d]Present address: Harvard University, Cambridge, MA 02138.
[e]Present address: Lawrence Berkeley Laboratory, Berkeley, CA 94720.
[f]Present address: Fermilab, Batavia, IL 60510.
[g]Present address: Northwestern University, Evanston, IL 60208.
[h]Present address: Lawrence Livermore National Laboratory, Livermore, CA 94550.

We present the first next-to-leading-order QCD analysis of neutrino charm production, using a sample of 6090 ν_μ- and $\overline{\nu}_\mu$-induced opposite-sign dimuon events observed in the CCFR detector at the Fermilab Tevatron. We find that the nucleon strange quark content is suppressed with respect to the non-strange sea quarks by a factor $\kappa = 0.477 \, ^{+\,0.063}_{-\,0.053}$, where the error includes statistical, systematic and QCD scale uncertainties. In contrast to previous leading order analyses, we find that the strange sea x-dependence is similar to that of the non-strange sea, and that the measured charm quark mass, $m_c = 1.70 \pm 0.19$ GeV/c^2, is larger and consistent with that determined in other processes. Further analysis finds that the difference in x-distributions between $xs(x)$ and $x\overline{s}(x)$ is small. A measurement of the Cabibbo-Kobayashi-Maskawa matrix element $|V_{cd}| = 0.232 \, ^{+\,0.018}_{-\,0.020}$ is also presented.

1. Introduction

Nucleon structure at high momentum transfers is characterized by parton distribution functions, which describe the proton and neutron in terms of quarks and gluons using the factorization theorems of Quantum Chromodynamics (QCD) [1]. These nucleon parton distributions are essential inputs when using perturbative calculations to predict high energy processes involving nucleons, such as those at the Tevatron collider and the planned LHC. The ability to consistently predict such processes using one set of universal parton distributions is an important test of QCD as the theory of the strong interactions. Neutrino-nucleon deep-inelastic scattering is particularly suited for measuring the parton densities due to the neutrino's ability to resolve the flavor of the nucleon constituents. Furthermore, neutrino scattering is an effective way to study the dynamics of heavy quark production, due to the light to heavy quark transition at the charged current vertex. In particular, neutrino charm production can be used to isolate the nucleon strange quark distributions, $xs(x)$ and $x\overline{s}(x)$.

We present the first next-to-leading-order (NLO) QCD analysis of neutrino and antineutrino production of charmed quarks including the first direct determination of the strange quark distribution defined at NLO. The order of the strange quark distribution from this analysis matches that of recent global nucleon structure analyses, like those of CTEQ [2] and MRS [3]. Since the data presented here provide the most sensitive constraints on the strange quark distribution, these results should become important ingredients in future global parton distribution fits.

In addition, we present measurements of the Cabibbo-Kobayashi-Maskawa (CKM) matrix element $|V_{cd}|$ and the mass of the charm quark m_c. The charm quark mass from this analysis is directly comparable with m_c measurements derived from NLO analyses of other processes. Such comparisons are a test of the perturbative QCD phenomenology for heavy quarks. Neutrino production of charm off nucleon d quarks provides a direct determination of the product $|V_{cd}|^2 B_c$, where B_c is the weighted average of the semileptonic branching ratios of the charmed hadrons produced. $|V_{cd}|$ is isolated by including an estimate of B_c using data from other experiments, including a re-analysis of Fermilab neutrino-emulsion data.

The signature for the production of charmed quarks in neutrino- and antineutrino-nucleon scattering is the presence of two oppositely-signed muons. In the case of neutrino scattering, the underlying process is a neutrino interacting with an s or d quark, producing a charm quark that fragments into a charmed hadron. The charmed hadron's semileptonic decay produces a second muon of opposite sign from the first.

$$\begin{aligned} \nu_\mu \; + \; \mathrm{N} \; \longrightarrow \; \mu^- \; + \; c \; + \; \mathrm{X} & \\ \hookrightarrow \; \mu^+ \; + \; \nu_\mu & \end{aligned}$$

The analogous process with an incident antineutrino proceeds through an interaction with

an $\overline{s}$ or $\overline{d}$ antiquark, again leading to oppositely-signed muons in the final state.

$$\begin{aligned} \overline{\nu}_\mu \ + \ \mathrm{N} \ \longrightarrow \ \mu^+ \ + \ \overline{c} \ + \ \mathrm{X} \\ \hookrightarrow \ \mu^- \ + \ \overline{\nu}_\mu \end{aligned}$$

2. The CCFR detector and event selection

The dimuon data were accumulated during two runs, E744 and E770, with the Chicago-Columbia-Fermilab-Rochester (CCFR) detector at the Fermilab Tevatron Quad-Triplet neutrino beam. This wide-band beam was composed of ν_μ and $\overline{\nu}_\mu$ with energies up to 600 GeV and a flatter energy spectrum than characteristic of horn-focused neutrino beams. In the CCFR detector [4, 5], neutrino interactions occur in the 690 ton unmagnetized steel-scintillator target-calorimeter, which is instrumented with drift chambers for muon tracking. The calorimeter's hadronic energy resolution is $\sigma/E = 0.85/\sqrt{E}$. The target is followed by a solid-iron toroidal magnetic spectrometer, which identifies muons and measures their momenta with a resolution $\Delta p = 0.11p$.

The detector measures p_{μ_1} and p_{μ_2}, the momenta of the two muons, θ_{μ_1} and θ_{μ_2}, the angles of the muons with respect to the neutrino beam axis, and $E_{\rm had}^{\rm vis}$, the energy of the hadronic system. Muon 1 is labeled as the leading muon, defined as the one emerging from the leptonic vertex, using a procedure described below. The visible energy in a dimuon event, $E_{\rm vis} = E_{\mu_1} + E_{\mu_2} + E_{\rm had}^{\rm vis}$, misses the energy of the decay neutrino. Therefore, we make the distinction between the *visible* quantities—quantities derived directly from measurement—and the *physical* quantities, which are inferred on average by correcting distributions of the visible quantities using the Monte Carlo simulation described below. Variables commonly used to describe deep inelastic scattering are: $Q^2_{\rm vis} = 4E_{\rm vis}E_{\mu_1}\sin^2(\theta_{\mu_1}/2)$, the negative square of the four-momentum transfer, $x_{\rm vis} = Q^2_{\rm vis}/[2M(E_{\rm had}^{\rm vis} + E_{\mu_2})]$, the Bjorken scaling variable, where M is the nucleon mass, $y_{\rm vis} = (E_{\rm had} + E_{\mu_2})/E_{\rm vis}$, the inelasticity, and $W^2_{\rm vis} = M^2 + Q^2_{\rm vis}(1/x_{\rm vis} - 1)$, the invariant mass squared of the hadronic system.

In the experiment, charged-current single muon events are required to have $E_{\rm vis} > 30$ GeV, $E_{\rm had}^{\rm vis} > 10$ GeV, $Q^2_{\rm vis} > 1$ GeV^2/c^2 and $p_{\mu_1} > 9$ GeV/c. Dimuon events are selected by making the further requirement that the second muon has $p_{\mu_2} > 5$ GeV/c and that both muons have $\theta_\mu < 0.250$ rad. The second muon's momentum is measured in the magnetic spectrometer whenever possible, otherwise it is determined from the muon's range in the target. In order to reduce non-prompt sources of second muons, events in which muon 2 does not reach the toroid must also satisfy $E_{\rm had}^{\rm vis} < 130$ GeV. The final dimuon sample contains 6090 events and is characterized by $\langle E_{\rm vis}\rangle = 192$ GeV, $\langle W^2_{\rm vis}\rangle = 168$ GeV^2/c^2, $\langle Q^2_{\rm vis}\rangle = 25.5$ GeV^2/c^2, and $\langle x_{\rm vis}\rangle = 0.15$. Results from a leading-order analysis of this data sample were reported previously [6].

3. Differential cross section

The differential cross section for dimuon production is expressed generally as

$$\frac{d^3\sigma(\nu_\mu N \to \mu^-\mu^+ X)}{d\xi\, dy\, dz} = \frac{d^2\sigma(\nu_\mu N \to cX)}{d\xi\, dy}\, D(z)\, B_c(c \to \mu^+ X), \tag{1}$$

where the function $D(z)$ describes the hadronization of charmed quarks and B_c is the weighted average of the semi-leptonic branching ratios of the charmed hadrons produced in neutrino interactions.

The heavy charm quark introduces an energy threshold in the charm production rate. This is a kinematic effect for which ξ, the momentum fraction of the struck quark, is related to the Bjorken scaling variable x, through the expression [7]

$$\xi = \left(\frac{1}{2x} + \sqrt{\frac{1}{4x^2} + \frac{M^2}{Q^2}}\right)^{-1} \frac{Q^2 - m_s^2 + m_c^2 + \Delta}{2Q^2}, \tag{2}$$

where m_c is the charm quark mass and m_s refers to the initial state quark mass, either the strange quark or the down quark, and $\Delta = \Delta(-Q^2, m_s^2, m_c^2)$ is the triangle function, defined by $\Delta(a,b,c) \equiv \sqrt{a^2+b^2+c^2-2(ab+bc+ca)}$. The full expression for ξ can be simplified by neglecting the small effect of the initial state quark mass to yield

$$\xi = x\left(1 + \frac{m_c^2}{Q^2}\right)\left(1 - \frac{x^2M^2}{Q^2}\right). \tag{3}$$

Relating ξ and x through the charm quark mass is referred to as slow-rescaling [8].

At leading order (LO) charm is produced by scattering directly off of strange and down quarks in the nucleon. The LO differential cross section for an isoscalar target, neglecting target mass effects, is given by:

$$\begin{aligned}\left\{\frac{d^2\sigma(\nu_\mu N \to cX)}{d\xi\, dy}\right\}_{LO} &= \frac{G^2 M E_\nu}{\pi(1+Q^2/M_W^2)^2}\, \{\, [\xi u(\xi,\mu^2) + \xi d(\xi,\mu^2)]\, |V_{cd}|^2 \\ &\quad + 2\xi s(\xi,\mu^2)\, |V_{cs}|^2 \,\} \left(1 - \frac{m_c^2}{2ME_\nu\xi}\right),\end{aligned} \tag{4}$$

where $\xi u(\xi,\mu^2)$, $\xi d(\xi,\mu^2)$ and $\xi s(\xi,\mu^2)$ represent the momentum distributions of the u, d and s quarks within the proton (the corresponding $\overline{\nu}_\mu$ process has the quarks replaced by their antiquark partners) and $|V_{cd}|$ and $|V_{cs}|$ are the CKM matrix elements. The dependence of the parton distributions on the scale μ^2 is specified by QCD [9]. In the leading order analysis of Reference [6], Callan-Gross violation is included by replacing the term $[1 - m_c^2/(2ME_\nu\xi)]$ in Equation (4) with $\{[1 + R_L(\xi,\mu^2)]\ [1 + (2M\xi/Q)^2]^{-1}$ $[1 - y - Mxy/(2E)]\ + xy/\xi\}$, and using external measurements of the structure function

$R_L(\xi, \mu^2)$ [10]. In the NLO formalism, violation of the Callan-Gross relation emerges as a consequence of QCD.

The LO expression illustrates the sensitivity of the process to the strange quark sea. Charm (anticharm) production from scattering off d ($\overline{d}$) quarks is Cabibbo suppressed. In the case of charm produced by neutrinos, approximately 50% is due to scattering from s quarks, even though the d quark content of the proton is approximately ten times larger. In the case of antineutrino scattering, where $\overline{d}$ quarks from the sea contribute, roughly 90% is due to scattering off $\overline{s}$ quarks.

Because neutrino charm production has a large sea quark component at leading-order, the next-to-leading-order gluon-initiated contributions are significant [11]. The size of the gluon distribution, which is an order of magnitude larger than the sea quark distribution, compensates for the extra power of α_S involved in the gluon-initiated diagram. The NLO quark-initiated diagrams, shown in Figure 1b, in which a gluon is radiated, also enter the perturbative expansion at $\mathcal{O}(\alpha_S)$, but the contributions of these diagrams to the cross section are not enhanced by large underlying parton distributions. Calculations including the next-to-leading-order formalism have recently become available [12, 13, 14] and lead to the analysis in this Letter.

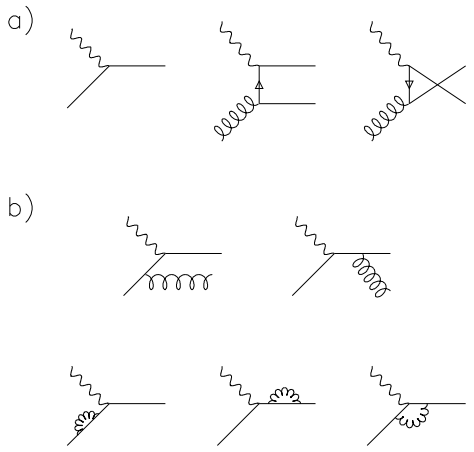

Figure 1: Mechanisms that contribute to neutrino production of charm up to $\mathcal{O}(\alpha_S)$. **a)** The dominant diagrams: the leading-order quark-initiated diagram, and the t channel and u channel gluon-initiated diagrams, respectively. **b)** The radiative-gluon and self-energy diagrams.

4. Monte Carlo simulation

Information about the strange sea, the charm quark mass, and the branching ratio is extracted by comparing the $x_{\rm vis}$ and $E_{\rm vis}$ distributions of the data to theoretical expectations contained in a Monte Carlo simulation. The Monte Carlo program models the dependence of these physics parameters as well as the effects of detector acceptance, resolution smearing, and missing energy associated with the charmed particle decay. Dimuon Monte Carlo event generation proceeds by using a simulated sample of charged-current single muon events and demanding that the hadronic system contains a second muon from charm decay. The single muon Monte Carlo sample is normalized to the charged-current data sample, ensuring that the Monte Carlo energy spectrum exactly models that of the data.

The species of charmed particles produced in neutrino interactions as a function of neutrino energy was measured by Fermilab E531 [15]. With an $E_\nu > 30$ GeV cut, the production is dominated by charged and neutral D mesons. Fragmentation to D's in the Monte Carlo simulation is parameterized by the fragmentation function of Collins and Spiller [16], $D(z) = N\left[(1-z)/z + \epsilon(2-z)/(1-z)\right](1+z)^2[1-(1/z)-\epsilon/(1-z)]^{-2}$, where $z = p_D/p_D^{\rm max}$ is the fraction of its maximum momentum that the D meson carries and ϵ is a free parameter. The parameter ϵ in the fragmentation model is fit by using the distribution of $z_{\rm vis} = E_{\mu_2}/(E_{\mu_2} + E_{had})$.

The dimuon events are divided into those from incident ν_μ or $\bar{\nu}_\mu$ by a separation procedure that assumes that the leading muon has larger transverse momentum with respect to the direction of the hadron shower than the muon from the charmed hadron decay. This procedure separates the sample into 5030 ν_μ-induced events and 1060 $\overline{\nu}_\mu$-induced events. The largest uncertainty in this procedure is due to the knowledge of the charm meson $p_\perp$ distribution. For this study we parameterize the $p_\perp$ distribution by $d{\rm n}/dp_\perp^2 \propto e^{-\beta p_\perp^2}$ and use the Fermilab E531 emulsion data [15] with $W^2 > 30$ GeV^2/c^2 to determine $\beta = 1.21 \pm 0.34$. Using this method, the separation procedure is found to misidentify $5.8 \pm 0.4\%$ of the ν events and $7.3 \pm 0.4\%$ of the $\overline{\nu}$ events.

The charm-initiated dimuon signal is contaminated by non-prompt pion and kaon decay. The high-density calorimeter minimizes this contamination due to the short interaction length of the detector. A combination of hadronic test beam muoproduction data and Monte Carlo simulations predicts a small π/K decay background of 797 ± 118 ν_μ and 118 ± 25 $\overline{\nu}_\mu$ events [17].

To calculate the probability of producing charm, we employ the NLO QCD charm production differential cross section calculation of Aivazis, Collins, Olness and Tung [12], including the Born and gluon-fusion diagrams, shown in Figure 1a. These are the leading contributions to charm production. The calculation is performed in the $\overline{\rm MS}$ scheme. The factorization scale in the calculation is chosen to be $\mu = 2p_\perp^{\rm max}$, where

$p_\perp^{\max} = \Delta(W^2, m_c^2, M^2)/\sqrt{4W^2}$ is the maximum available transverse momentum of the initial state quark coming from the gluon splitting, or equivalently of the final state charm quark, for the given kinematic variables x and Q^2. The renormalization scale is chosen to equal the factorization scale. We discuss the uncertainty due to the choice of these scales below. Electromegnetic radiative corrections to the cross section are calculated using the method of Bardin *et al.* [18].

The finite momentum cut on the second muon limits the acceptance of events attributable to gluon-initiated production,

$$W^+ g \to c\overline{s}.$$

Gluon-initiated production of charm proceeds through both the t and u channels as shown in Figure 1a. While these diagrams are quantum mechanically equivalent, they dominate different regions of phase space. In the t channel, the gluon splits into an $s\overline{s}$ pair and the c quark emerges from the W-boson vertex. In the u channel, the legs of the c and $\overline{s}$ quarks are crossed—the gluon splits into a $c\overline{c}$ pair and the $\overline{s}$ quark emerges from the W-boson vertex.

In the W-boson–gluon center of mass frame, the c quark is produced at an angle θ_c^* relative to the W-boson direction. The production angle is related to the momentum of the c quark in the lab, and hence with p_{μ_2}. When θ_c^* is small—t channel dominance—the c quark carries most of the W-boson momentum. As θ_c^* approaches π—u channel dominance—the c quark emerges with little momentum in the lab. Consequently, events with large θ_c^* are less likely to produce a second muon with $p_{\mu_2} > 5$ GeV/c.

An acceptance correction due to this effect is determined by folding the calculated squared production amplitude for producing charm at angle θ_c^* with the experimental acceptance. To determine the experimental acceptance, the ability of events with finite θ_c^* to pass the 5 GeV/c p_{μ_2} cut is compared to that when the events are generated with $\theta_c^* = 0$. We find that this relative acceptance drops to near zero at $\theta_c^* = \pi$, and is about 74% at $\theta_c^* = \pi/2$. Integrating over the calculated squared production amplitude, which peaks in the forward and backward directions, the overall t–u channel acceptance correction for gluon-initiated production is $60 \pm 10\%$. The effect of this acceptance correction is small but not insignificant; for example, it shifts the value of m_c determined from the fit described below by $+0.07$ GeV/c^2.

Measurements of the F_2 and xF_3 structure functions by CCFR [19, 20] are used to determine the singlet and the non-singlet quark distributions, $xq_{SI}(x,\mu^2) = xq(x,\mu^2) + x\overline{q}(x,\mu^2)$ and $xq_{NS}(x,\mu^2) = xq(x,\mu^2) - x\overline{q}(x,\mu^2)$, respectively, and the gluon distribution, $xg(x,\mu^2)$ [21]. These distributions are obtained from next-to-leading-order QCD fits to the structure function data [22] using the QCD evolution programs of Duke and Owens [23].

To resolve the strange component of the quark sea, the singlet and non-singlet quark distributions are separated by flavor. Insofar as isospin is a good symmetry, our experiment is insensitive to the exact form of the up and down valence and sea quark distributions, because the neutrino target is nearly isoscalar. An isoscalar correction accounts for the 5.67% neutron excess in the target.

The proton valence quark content, $xq_V(x,\mu^2) = xq_{NS}(x,\mu^2)$, is parameterized by

$$\begin{aligned} xq_V(x,\mu^2) &= xu_V(x,\mu^2) + xd_V(x,\mu^2), \\ xd_V(x,\mu^2) &= A_d(1-x)xu_V(x,\mu^2), \end{aligned} \tag{5}$$

where the shape difference for $xd_V(x)$ better fits charged-lepton scattering measurements of $F_2^{\rm n}/F_2^{\rm p}$ [24]. A_d is fixed by demanding that the ratio of the number of d to u valence quarks in the proton is 1/2.

The non-strange quark and antiquark components of the sea are assumed to be symmetric, so that $x\overline{u}(x,\mu^2) = xu_S(x,\mu^2)$, $x\overline{d}(x,\mu^2) = xd_S(x,\mu^2)$. The isoscalar correction is applied assuming $x\overline{u}(x,\mu^2) = x\overline{d}(x,\mu^2)$. The strange component of the quark sea is allowed to have a different magnitude and shape from the non-strange component. The strange quark content is set by the parameter

$$\kappa = \frac{\int_0^1 [xs(x,\mu^2) + x\overline{s}(x,\mu^2)]\,dx}{\int_0^1 [x\overline{u}(x,\mu^2) + x\overline{d}(x,\mu^2)]\,dx}, \tag{6}$$

where $\kappa = 1$ would indicate a flavor SU(3) symmetric sea. The shape of the strange quark distribution relates to that of the non-strange sea by a shape parameter α, where $\alpha = 0$ would indicate that the strange sea has the same x dependence as the non-strange component of the quark sea. Shape parameters are defined for each of the two fits below. In the first fit the strange quark and antiquark distributions are assumed to be the same; in the second fit $xs(x,\mu^2)$ and $x\overline{s}(x,\mu^2)$ are fit separately.

4.1 $xs(x,\mu^2) = x\overline{s}(x,\mu^2)$ fit

This fit assumes that $xs(x,\mu^2)$ and $x\overline{s}(x,\mu^2)$ are the same. The sea quark distributions are parameterized by:

$$\begin{aligned} x\overline{q}(x,\mu^2) &= 2\left[\frac{x\overline{u}(x,\mu^2) + x\overline{d}(x,\mu^2)}{2}\right] + xs(x,\mu^2), \\ xs(x,\mu^2) &= A_s(1-x)^\alpha \left[\frac{x\overline{u}(x,\mu^2) + x\overline{d}(x,\mu^2)}{2}\right], \end{aligned} \tag{7}$$

where A_s is defined in terms of κ and α.

A χ^2 minimization is performed to find the strange sea parameters κ and α, the values of B_c and m_c, and the fragmentation parameter ϵ, by fitting to the $x_{\rm vis}$, $E_{\rm vis}$ and $z_{\rm vis}$

distributions of the dimuon data, projections of which are shown in Figure 2. Taking $|V_{cd}| = 0.221 \pm 0.003$ and $|V_{cs}| = 0.9743 \pm 0.0008$ [25] as input values and using the Collins-Spiller fragmentation function, the extracted NLO parameters with their statistical and systematic errors are presented in the first line of Table 1. In this primary fit, the uncertainties due to fragmentation are included in the statistical errors of all of the parameters. The value of $\chi^2 = 52.2$ for 65 degrees of freedom suggests excellent agreement between the data and the NLO theoretical model.

Our previous LO results [6], which were found by fitting to the $x_{\rm vis}$ and $E_{\rm vis}$ distributions of the same data sample and using the Peterson fragmentation function [26], $D(z) = N\{\, z[1 - (1/z) - \epsilon_P/(1-z)]^2 \,\}^{-1}$ with $\epsilon_P = 0.20$, are listed in the third line of Table 1. For comparison with these results, Table 1 includes the NLO parameters determined using the same fit procedure. The two fits using the Peterson fragmentation function include the uncertainty due to fragmentation in the systematic errors of all of the parameters.

	Fragmentation	χ^2/dof	κ	α	B_c	m_c (GeV/c^2)
NLO fit	Collins-Spiller	52.2/65	$0.477\ ^{+0.046\ +0.023}_{-0.044\ -0.024}$	$-0.02\ ^{+0.60\ +0.28}_{-0.54\ -0.26}$	$0.1091\ ^{+0.0082\ +0.0063}_{-0.0074\ -0.0051}$	$1.70\ \pm 0.17\ ^{+0.09}_{-0.08}$
	$\epsilon = 0.81 \pm 0.14$					
NLO fit	Peterson	41.2/46	$0.468\ ^{+0.061\ +0.024}_{-0.046\ -0.025}$	$-0.05\ ^{+0.46\ +0.28}_{-0.47\ -0.26}$	$0.1047\ \pm 0.0076\ ^{+0.0065}_{-0.0052}$	$1.69\ \pm 0.16\ ^{+0.12}_{-0.10}$
	$\epsilon_P = 0.20 \pm 0.04$					
LO fit	Peterson	42.5/46	$0.373\ ^{+0.048}_{-0.041} \pm 0.018$	$2.50\ ^{+0.60\ +0.36}_{-0.55\ -0.25}$	$0.1050 \pm 0.007 \pm 0.005$	$1.31\ ^{+0.20\ +0.12}_{-0.22\ -0.11}$
Ref. [6]	$\epsilon_P = 0.20 \pm 0.04$					

Table 1: Next-to-leading-order and leading-order fit results, assuming $xs(x) = x\overline{s}(x)$. Errors are statistical and systematic, except that the errors on the fragmentation parameters are statistical only.

Estimates of the systematic uncertainties are obtained by varying model parameters within errors and are itemized in Table 2.

Parton distributions are defined to a given order and scheme in QCD. Therefore, the magnitude of a given parton distribution differs between leading-order and next-to-leading-order. At NLO, the nucleon strange quark content is found to be $\kappa = 0.477\,^{+0.051}_{-0.050}$, indicating that the sea is not SU(3) symmetric—qualitatively the same result as from the LO analysis. The strange quark content may alternatively be given by

$$\eta = \frac{\int_0^1 [xs(x,\mu^2) + x\overline{s}(x,\mu^2)]\,dx}{\int_0^1 [xu(x,\mu^2) + xd(x,\mu^2)]\,dx}, \tag{8}$$

so that by comparing to the total non-strange quark content, η is less sensitive to changes in the determination of the sea quark content alone. At $\mu^2 = 22.2$ GeV^2/c^2 the ratio of

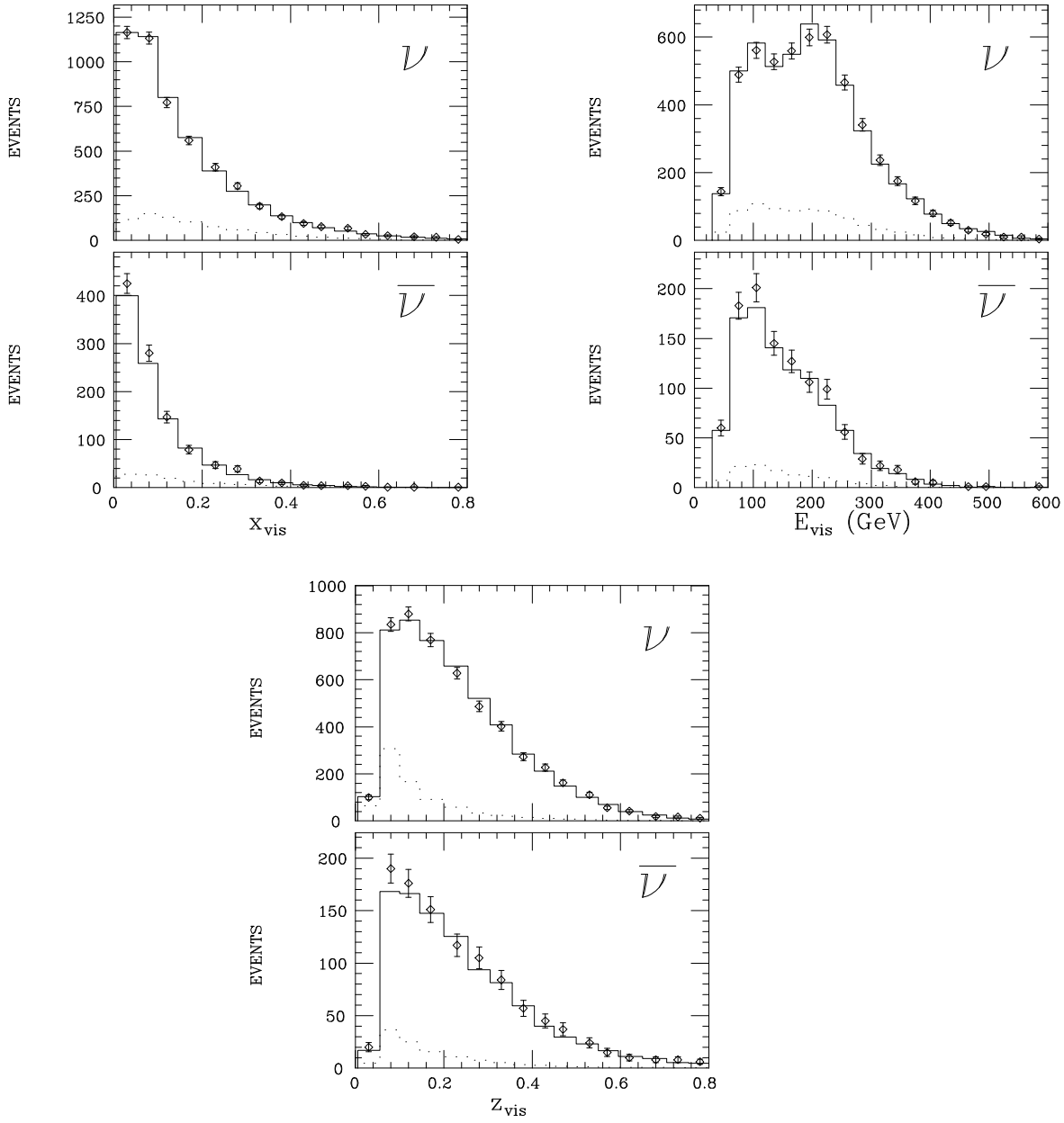

Figure 2: $x_{\rm vis}$, $E_{\rm vis}$ and $z_{\rm vis}$ distributions for ν- and $\overline{\nu}$-induced dimuon events. Data are given by the points and the solid histogram is the result of fitting the dimuon event simulation. The dotted histogram is the background contribution to the former from pion and kaon decay.

source of uncertainty	κ	α	B_c	m_c
π/K background	$^{+\,0.0010}_{-\,0.0022}$	$^{+\,0.150}_{-\,0.160}$	$^{-\,0.0031}_{+\,0.0027}$	$^{+\,0.006}_{-\,0.003}$
energy scale	$^{-\,0.0051}_{+\,0.0078}$	$^{-\,0.048}_{+\,0.059}$	$^{+\,0.0028}_{-\,0.0002}$	$^{+\,0.031}_{-\,0.057}$
relative calibration	$^{-\,0.0059}_{+\,0.0020}$	$^{+\,0.115}_{-\,0.077}$	$^{+\,0.0013}_{-\,0.0002}$	$^{+\,0.031}_{-\,0.007}$
detection efficiency $\pm 1\%$	$^{-\,0.0070}_{+\,0.0021}$	$^{+\,0.044}_{-\,0.003}$	$^{+\,0.0022}_{-\,0.0012}$	$^{-\,0.007}_{+\,0.013}$
$\nu - \overline{\nu}$ mis-id	$^{+\,0.0014}_{-\,0.0032}$	$^{-\,0.042}_{+\,0.006}$	$^{+\,0.0009}_{-\,0.0014}$	$^{+\,0.036}_{-\,0.030}$
F_2 and xF_3	$^{+\,0.0143}_{-\,0.0068}$	$^{+\,0.084}_{-\,0.114}$	$^{+\,0.0024}_{-\,0.0019}$	$^{+\,0.053}_{-\,0.017}$
$xq_{SI}(x)$, $xq_{NS}(x)$ and $xg(x)$	$^{+\,0.0110}_{-\,0.0110}$	$^{+\,0.180}_{-\,0.180}$	$^{+\,0.0009}_{-\,0.0009}$	$^{+\,0.038}_{-\,0.038}$
$\lvert V_{cs}\rvert$ and $\lvert V_{cd}\rvert$	$^{+\,0.0095}_{-\,0.0099}$	$^{-\,0.024}_{+\,0.031}$	$^{-\,0.0028}_{+\,0.0032}$	$^{-\,0.011}_{+\,0.014}$
t–u channel accep. corr.	$^{-\,0.0135}_{+\,0.0052}$	$^{-\,0.009}_{+\,0.062}$	$^{-\,0.0002}_{+\,0.0010}$	$^{-\,0.020}_{+\,0.008}$

Table 2: Sources of systematic uncertainty in the determination of the fit parameters.

antiquarks to quarks in the nucleon at NLO is found to be $\int dx x\overline{q}(x,\mu^2)/\int dx x q(x,\mu^2) = \overline{Q}/Q = 0.245 \pm 0.005$ and thereby the strange quark content with respect to the non-strange quarks is

$$\eta = 0.099 \pm 0.008 \pm 0.004\,{}^{-\,0.003}_{+\,0.006}. \tag{9}$$

Since a nonzero value of α would indicate a shape difference between $x\overline{q}(x)$ and $xs(x)$, the value $\alpha = -0.02\,{}^{+\,0.66}_{-\,0.60}$ indicates no shape difference at NLO. At leading order, we find the strange quarks softer than the overall quark sea by a factor $(1-x)^\alpha$ with $\alpha = 2.5 \pm 0.7$. The difference in α between NLO and LO is attributable to the NLO $x\overline{q}(x)$ being softer than its LO counterpart, as shown in Figure 3. Figure 4 shows the NLO and LO $xs(x)$, again indicating that the NLO distribution is larger in magnitude and softer than its LO counterpart.

The strange quark distribution from the $xs(x,\mu^2) = x\overline{s}(x,\mu^2)$ fit is tabulated in Table 3 for a few values of x and μ^2 and is plotted at $\mu^2 = 4$ GeV^2/c^2 in Figure 4. The distribution can be parameterized by a function of the form $a\,(1-x)^b\,x^{-c}$. The values of the coefficients a, b and c are tabulated in Table 4.

The charm quark mass parameter from the NLO fit is 1.70 ± 0.19 GeV/c^2, which differs from the leading-order result, indicating the marked dependence of m_c on the order to which the analysis is done. The NLO value of m_c can be more consistently compared with measurements derived from other processes involving similar higher-order perturbative QCD calculations. A photon-gluon-fusion analysis of photoproduction data finds $m_c = 1.74\,{}^{+0.13}_{-0.18}$ [27].

The values of B_c from the NLO and LO fits are consistent, providing a good check

μ^2 (GeV^2/c^2)	x	$xs(x,\mu^2)$
1.0	0.01	$0.126 \pm 0.012 \pm 0.006\ ^{+\,0.008}_{-\,0.004}$
	0.05	$0.097 \pm 0.008 \pm 0.004\ ^{+\,0.006}_{-\,0.003}$
	0.10	$0.068 \pm 0.005 \pm 0.003\ ^{+\,0.004}_{-\,0.002}$
	0.20	$0.032 \pm 0.003 \pm 0.001\ ^{+\,0.002}_{-\,0.001}$
4.0	0.01	$0.178 \pm 0.016 \pm 0.008\ ^{+\,0.011}_{-\,0.005}$
	0.05	$0.111 \pm 0.009 \pm 0.005\ ^{+\,0.007}_{-\,0.003}$
	0.10	$0.072 \pm 0.005 \pm 0.003\ ^{+\,0.004}_{-\,0.002}$
	0.20	$0.030 \pm 0.003 \pm 0.001\ ^{+\,0.002}_{-\,0.001}$
20.0	0.01	$0.229 \pm 0.020 \pm 0.010\ ^{+\,0.014}_{-\,0.007}$
	0.05	$0.122 \pm 0.010 \pm 0.005\ ^{+\,0.007}_{-\,0.004}$
	0.10	$0.073 \pm 0.006 \pm 0.003\ ^{+\,0.004}_{-\,0.002}$
	0.20	$0.028 \pm 0.003 \pm 0.001\ ^{+\,0.002}_{-\,0.001}$
100.0	0.01	$0.271 \pm 0.024 \pm 0.012\ ^{+\,0.017}_{-\,0.008}$
	0.05	$0.128 \pm 0.010 \pm 0.005\ ^{+\,0.008}_{-\,0.004}$
	0.10	$0.072 \pm 0.006 \pm 0.003\ ^{+\,0.004}_{-\,0.002}$
	0.20	$0.026 \pm 0.003 \pm 0.001\ ^{+\,0.002}_{-\,0.001}$

Table 3: Values of $xs(x,\mu^2)$, defined at NLO using the $\overline{\rm MS}$ renormalization scheme, from the $xs(x,\mu^2) = x\overline{s}(x,\mu^2)$ fit. The first error is statistical, the second is experimental systematic and the third is due to QCD scale uncertainty.

of the fit procedure and the physics model. This value is constrained by neutrino charm production at $x > 0.3$ where the valence d quark contribution dominates, and thus is independent of the strange and other sea quark distributions. The value of $B_c = 0.109^{+0.010}_{-0.007}$ agrees with an indirect determination, $B_c^{\rm I} = 0.099 \pm 0.012$, which is described in section 5.

As with all applications of perturbative QCD, a theoretical uncertainty is associated with the choice of factorization and renormalization scales. Some scale dependence is unavoidable for any calculation done to finite order in α_S. The μ^2 scale is interpreted as setting the boundary between the collinear and noncollinear regions of the $p_\perp$ integration over the final states. Therefore, a scale proportional to $p_\perp^{\rm max}$ is suggested by the authors of

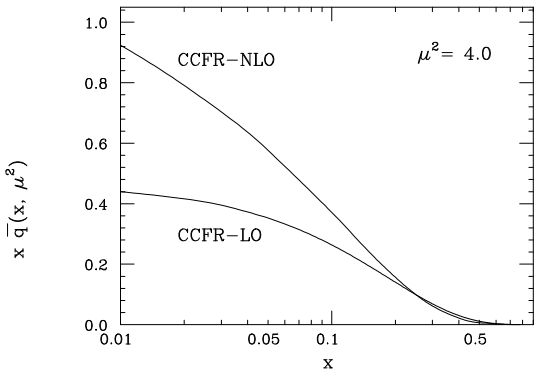

Figure 3: The quark sea distribution $x\overline{q}(x, \mu^2 = 4.0\ \mathrm{GeV}^2/\mathrm{c}^2)$ determined at next-to-leading order and leading order.

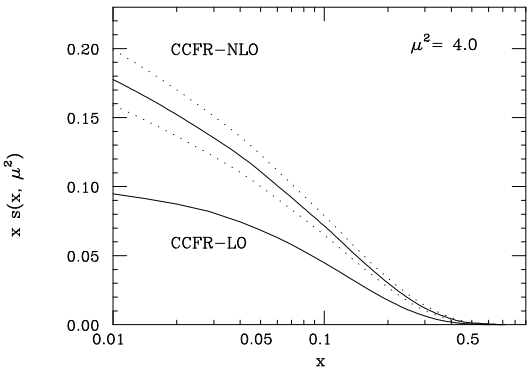

Figure 4: The strange quark distribution $xs(x, \mu^2 = 4.0\,\mathrm{GeV}^2/\mathrm{c}^2)$ determined at next-to-leading order (described in section 4.1) and leading order. The band around the NLO curve indicates the $\pm 1\sigma$ uncertainty in the distribution.

μ^2 GeV^2/c^2	a	b	c
1.0	0.135	6.48	0.000
10.0	0.117	6.67	0.096
20.0	0.107	6.98	0.164
100.0	0.100	7.28	0.210

Table 4: The coefficients a, b and c from the parameterization of $xs(x, \mu^2)$ using the form $a(1-x)^b x^{-c}$, as described in the text.

Ref. [11, 28]. Figure 5 shows the scale dependence of the differential cross section, where the abscissa is in units of $p_\perp^{\max}$. The scale dependence is weak for μ values above one unit of $p_\perp^{\max}$, and there is a stronger scale dependence when μ is below this value. We choose $\mu = 2p_\perp^{\max}$ and find the scale uncertainty by varying μ between $p_\perp^{\max}$ and $3p_\perp^{\max}$. Fit results with various choices of the common factorization and renormalization scale are presented in Table 5. The χ^2 values for these fits—all with 65 degrees of freedom—indicate that the data favor μ^2 scales with smaller magnitudes. It should be noted that the values of the fit parameters are fairly insensitive to the choice of scale.

choice of scale, μ^2	χ^2	κ	α	B_c	m_c (GeV/c^2)
$(\,p_\perp^{\rm max})^2$	50.4	0.513	0.18	0.0987	1.71
$(2\,p_\perp^{\rm max})^2$	52.2	0.477	-0.02	0.1091	1.70
$(3\,p_\perp^{\rm max})^2$	54.4	0.460	-0.10	0.1142	1.68
Q^2	51.7	0.423	-0.37	0.1074	1.80
$(2Q)^2$	56.1	0.410	-0.46	0.1159	1.71
$(3Q)^2$	59.4	0.408	-0.54	0.1206	1.73
$Q^2 + m_c^2$	52.5	0.421	-0.03	0.1066	1.65
$4\,(Q^2 + m_c^2)$	57.1	0.409	-0.16	0.1154	1.64
$Q^2 + (2m_c)^2$	52.8	0.428	0.00	0.1068	1.62
$4\,[Q^2 + (2m_c)^2]$	57.3	0.415	-0.15	0.1161	1.63

Table 5: Central values of the fit parameters for various choices of the QCD scale μ^2. Each fit contains 65 degrees of freedom.

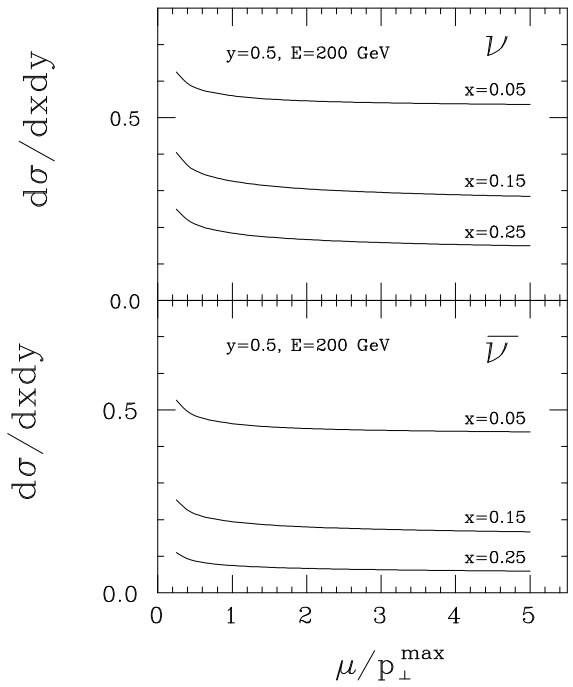

Figure 5: The μ^2 scale dependence of the differential cross section for neutrino and antineutrino production of charm, where μ^2 identifies the factorization and renormalization scales. The scale μ on the abscissa is in units of $p_\perp^{\max}$. For $E = 200$ GeV and $y = 0.5$, the $x = 0.05$, 0.15, 0.25 lines correspond to $p_\perp^{\max} = 6.6$, 6.2, 5.8 GeV/c, respectively.

4.2 $xs(x) \neq x\overline{s}(x)$ fit

Theoretical work has explored the possibility that the nucleon contains a sizable heavy quark component at moderate x—the possibility of so-called intrinsic heavy quark states within the nucleon [29]. Postulating intrinsic strange quark states leads to the prediction that the s quark momentum distribution will be harder than the $\overline{s}$ quark distribution [30]. We explore this possibility by performing a fit in which the momentum distributions of the s and $\overline{s}$ quarks are allowed to be different. For this study the sea quark distributions are parameterized by:

$$x\overline{q}(x,\mu^2) \;=\; 2\left(\frac{x\overline{u}(x,\mu^2)+x\overline{d}(x,\mu^2)}{2}\right)+\frac{xs(x,\mu^2)+x\overline{s}(x,\mu^2)}{2},$$

$$
\begin{aligned}
xs(x,\mu^2) &= A_s(1-x)^{\alpha}\left[\frac{x\overline{u}(x,\mu^2)+x\overline{d}(x,\mu^2)}{2}\right], \\
x\overline{s}(x,\mu^2) &= A'_s(1-x)^{\alpha'}\left[\frac{x\overline{u}(x,\mu^2)+x\overline{d}(x,\mu^2)}{2}\right].
\end{aligned} \tag{10}
$$

The s and $\overline{s}$ are constrained to have the same number

$$
\int_0^1 s(x,\mu^2)\,dx = \int_0^1 \overline{s}(x,\mu^2)\,dx. \tag{11}
$$

A_s and A'_s are defined in terms of κ, α and α'.

In order to reduce the number of free parameters, this fit constrains the average charmed hadron branching ratio to the value obtained from other measurements, $B_c^{\rm I} = 0.099 \pm 0.012$ (see Section 5.). We fit for four parameters: the strange quark parameters κ, α, and $\Delta\alpha = \alpha - \alpha'$ and the charm quark mass m_c. The result is:

$$
\begin{aligned}
\kappa &= 0.536 \pm 0.030 \pm 0.036\,{}^{-\,0.064}_{+\,0.098} \pm 0.009, \\
\alpha &= -0.78 \pm 0.40 \pm 0.56 \pm 0.98 \pm 0.50, \\
\Delta\alpha &= -0.46 \pm 0.42 \pm 0.36 \pm 0.65 \pm 0.17, \\
m_c &= 1.66 \pm 0.16 \pm 0.07\,{}^{+\,0.04}_{-\,0.01} \pm 0.01\ {\rm GeV/c^2},
\end{aligned} \tag{12}
$$

where the first error is statistical, the second is systematic, the third is due to the uncertainty in $B_c^{\rm I}$, and the fourth is the error due to μ^2 scale uncertainty.

The value of $\Delta\alpha = -0.46 \pm 0.85 \pm 0.17$ indicates that the momentum distributions of s and $\overline{s}$ are consistent and the difference in the two distributions is limited to $-1.9 < \Delta\alpha < 1.0$ at the 90% confidence level. This is the first quantitative comparison of the components of the s and $\overline{s}$ quark sea.

We also checked the assumption that the same average semileptonic branching ratio applies to the ν- and $\overline{\nu}$-induced samples. A two parameter fit finds the branching ratio of ν-induced events $B_c = 0.1147 \pm 0.0056$, and $\Delta B_c = B_c - B'_c = 0.011 \pm 0.011$, where B'_c is the branching ratio for $\overline{\nu}$-induced events and the errors are statistical only. The result indicates that there is no significant difference in the semileptonic decays of charmed particles and antiparticles at these energies.

5. $|V_{cd}|$ measurement

If the CKM matrix elements are not assumed, then the four parameter NLO fit in section 4.1 is performed by fitting α, m_c and the following products:

$$
\begin{aligned}
|V_{cd}|^2 B_c &= (5.34\,{}^{+\,0.38}_{-\,0.39}\,{}^{+\,0.27}_{-\,0.21}\,{}^{+\,0.25}_{-\,0.51}) \times 10^{-3}, \\
\frac{\kappa}{\kappa+2}|V_{cs}|^2 B_c &= (2.00 \pm 0.10\,{}^{+\,0.07}_{-\,0.05}\,{}^{+\,0.06}_{-\,0.14}) \times 10^{-2}.
\end{aligned} \tag{13}
$$

These combinations can be used to extract $|V_{cd}|^2$ and $\kappa|V_{cs}|^2$ when B_c is determined from other data. B_c is determined by combining the charmed particle semileptonic branching ratios measured at e^+e^- colliders [25] with the neutrino-production fractions measured by the Fermilab E531 neutrino-emulsion experiment [15]. Using an $E_{\rm vis} > 30$ GeV cut, E531 determined the following production fractions: $52 \pm 6\%$ D^0, $42 \pm 6\%$ D^+, $1 \pm 2\%$ D_s^+, and $5 \pm 3\%$ Λ_c^+. In the E531 analysis, events that could not be unambiguously identified as D^+ or D_s^+ were all categorized as D^+ events. To remove this small bias, a re-analysis was performed that included updated values of the charmed hadron lifetimes [31]. This re-analysis finds the following production fractions with an $E_{\rm vis} > 30$ GeV cut: $60 \pm 6\%$ D^0, $26 \pm 6\%$ D^+, $7 \pm 5\%$ D_s^+, and $7 \pm 4\%$ Λ_c^+. These production fractions are consistent with those measured by e^+e^- experiments [32].

We find $B_c^{\rm I} = 0.099 \pm 0.012$ and extract the value of the CKM matrix element

$$|V_{cd}| = 0.232 \, ^{+\,0.018}_{-\,0.020}, \tag{14}$$

where the error indicates all sources of uncertainty, including the μ^2 scale uncertainty. It compares very well with the PDG value, $|V_{cd}| = 0.221 \pm 0.003$, which is determined from measurements of the other matrix elements and the unitarity constraint on the CKM matrix assuming three generations. A measurement of $|V_{cs}|$ will be possible when an independent measurement of the strange sea content is available.

6. Summary

We have perfomed the first NLO QCD analysis of neutrino charm production and have measured the nucleon strange quark distribution and the electroweak parameters m_c and $|V_{cd}|$. We find:

$$\begin{aligned} m_c &= 1.70 \pm 0.19 \pm 0.02 \\ \kappa &= 0.477 \, ^{+\,0.051\ -\,0.017}_{-\,0.050\ +\,0.036} \\ \alpha &= -0.02 \, ^{+\,0.66\ +\,0.08}_{-\,0.60\ -\,0.20} \end{aligned} \tag{15}$$

where κ is the strange quark content with respect to the non-strange sea and α indicates a shape difference between the strange and non-strange sea, $xs(x) \propto (1-x)^\alpha$ $[x\overline{u}(x) + x\overline{d}(x)]/2$. The first error combines statistical and systematic errors in quadrature and the second is the uncertainty due to QCD μ^2 scale. This value of κ indicates that the quark sea is not flavor SU(3) symmetric. The relative shape parameter α is consistent with zero, indicating that there is no shape difference between the strange and non-strange components of the sea. The value of m_c obtained from the NLO analysis is consistent with that found in other processes.

Using an externally determined production weighted charmed hadron branching ratio, $B_c^{\rm I} = 0.099 \pm 0.012$, we measure the CKM matrix element

$$|V_{cd}| = 0.232 \, ^{+\,0.018}_{-\,0.020}. \tag{16}$$

We have also studied the possibility of a shape difference between the $xs(x)$ and $x\overline{s}(x)$ distributions. We find that

$$\Delta\alpha = \alpha - \alpha' = -0.46 \pm 0.85 \pm 0.17, \tag{17}$$

where α and α' are shape parameters for $xs(x)$ and $x\overline{s}(x)$, indicating no shape difference between the components of the strange quark sea. A shape difference is limited to $-1.9 < \alpha - \alpha' < 1.0$ at 90% confidence level.

The strange sea can also be inferred from a comparison of charged lepton and neutrino structure functions. To leading-order the lepton and neutrino structure functions are related by the "5/18ths rule," $F_2^{lN}/F_2^{\nu N} = 5/18\{\ 1 - 3/5[(s+\overline{s})/(q+\overline{q})]\ \}$, where the strange sea enters as a correction. Comparison of structure function measurements from CCFR (νFe) [19, 20] with those form SLAC (eD) [33], NMC [34] and BCDMS (μD) [35], shows good agreement for $x > 0.1$ but a small discrepancy is seen between the neutrino and muon results for lower x. The source of this disagreement is under investigation, but may be due to the extra axial vector component present in neutrino scattering [36]. In contrast, the recent global fits by the CTEQ Collaboration (CTEQ1 distributions) [2] have attributed the muon versus neutrino difference to an enhanced strange sea at low x.[1] This possibility is ruled out by the measurements presented here.

Acknowledgement

We thank M.A.G. Aivazis, F.I. Olness and W.-K. Tung for encouragement, useful discussions and for providing computer code of their cross section calculation. We thank the management and staff of Fermilab, and acknowledge the help of many individuals at our home institutions. S.R.M. acknowledges the support of the Alfred P. Sloan and Cottrell Foundations. This research was supported by the National Science Foundation and the Department of Energy of the United States, who should be credited for their continued support of basic research.

References

[1] J.C. Collins, D.E. Soper and G. Sterman, in: Perturbative Quantum Chromodynamics, ed. A.H. Mueller (World Scientific, Singapore, 1989).

[2] J. Botts *et al.* (CTEQ Collab.), Phys. Lett. B 304 (1993) 159.

[3] A.D. Martin, R.G. Roberts and W.J. Stirling, Phys. Lett. B 306 (1993) 145.

[1] The more recent CTEQ2 distributions include a preliminary version of the NLO strange sea results presented here, but do not account for the structure function discrepancy.

[4] W.K. Sakumoto *et al.* (CCFR Collab.), Nucl. Instrum. Methods Phys. Res. A 294 (1990) 179.

[5] B.J. King *et al.* (CCFR Collab.), Nucl. Instrum. Methods Phys. Res. A 302 (1991) 254.

[6] S.A. Rabinowitz *et al.* (CCFR Collab.), Phys. Rev. Lett. 70 (1993) 134.

[7] M.A.G. Aivazis, F.I. Olness and W.-K. Tung, MSU-HEP 93/15.

[8] R.M. Barnett, Phys. Rev. Lett. 36 (1976) 1163. H. Georgi and H.D. Politzer, Phys. Rev. D 14 (1976) 1829.

[9] V.N. Gribov and L.N. Lipatov, Sov. J. Nucl. Phys. 15 (1972) 438; G. Altarelli and G. Parisi, Nucl. Phys. B 126 (1977) 298.

[10] S. Dasu *et al.*, Phys. Rev. Lett. 61 (1988) 1061.

[11] M.A.G. Aivazis, F.I. Olness and W.-K. Tung, Phys. Rev. Lett. 65 (1990) 2339.

[12] M.A.G. Aivazis, J.C. Collins, F.I. Olness and W.-K. Tung, SMU-HEP/93-17.

[13] G. Kramer and B. Lampe, Z. Phys. C 54 (1992) 139.

[14] J.J. van der Bij and G.J. van Oldenborgh, Z. Phys. C 51 (1991) 477.

[15] N. Ushida *et al.* (E531 Collab.), Phys. Lett. B 206 (1988) 375; B 206 (1988) 380.

[16] P. Collins and T. Spiller, J. Phys. G 11 (1985) 1289.

[17] P.H. Sandler *et al.* (CCFR Collab.), Z. Phys. C 57 (1993) 1.

[18] D. Bardin and N. Shumeiko, Sov. J. Nucl. Phys. 29 (1979) 499.

[19] P.Z. Quintas *et al.* (CCFR Collab.), Phys. Rev. Lett. 71 (1993) 1307.

[20] W.C. Leung *et al.* (CCFR Collab.), Phys. Lett. B 317 (1993) 655.

[21] The parton distributions are parameterized at a reference scale μ_0^2 by $xq_{NS}(x,\mu_0^2) = A_{NS}x^{\eta_1}(1-x)^{\eta_2} + B_{NS}x^{\eta_3}$, $xq_{SI}(x,\mu_0^2) = xq_{NS}(x,\mu_0^2) + A_{\rm sea}(1-x)^{\eta_{\rm sea}}$ and $xg(x,\mu_0^2) = A_g(1-x)^{\eta_g}$, and evolved to all other values of μ^2 using the GLAP [9] evolution equations. A_{NS} is constrained by the fermion conservation sum rule $\int \frac{dx}{x} xq_{NS}(x) = 3$, and A_g is constrained by the momentum sum rule $\int dx\ [xq_{SI}(x) + xg(x)] = 1$. The final fit parameter is the strong coupling constant, given by $\Lambda_{\overline{\rm MS}}$, for a total of eight fit parameters. At $\mu_0^2 = 1$ GeV^2/c^2, the parameters are $\Lambda_{\overline{\rm MS}} = 0.210 \pm 0.021$ GeV/c, $\eta_1 = 0.947 \pm 0.027$, $\eta_2 = 3.81 \pm 0.059$, $\eta_3 = 0.405 \pm 0.047$, $B_{NS} = 0.0210 \pm 0.0039$, $A_{\rm sea} = 1.404 \pm 0.047$, $\eta_{\rm sea} = 6.49 \pm 0.22$, $\eta_g = 3.18 \pm 0.70$, where the errors are statistical only.

[22] W.G. Seligman *et al.* (CCFR Collab.), in: Proc. XXVIIIth Rencontre de Moriond: QCD and High Energy Hadronic Interactions (Les Arcs, March 1993), ed. J. Tran Thanh Van (Editions Frontieres, Gif-sur-Yvette, 1993) p. 39.

[23] D. Duke and J. Owens, Phys. Rev. D 30 (1984) 49.

[24] P. Amaudruz *et al.*, (NMC Collab.), Nucl. Phys. B 371 (1992) 3.

[25] K. Hikasa *et al.* (Particle Data Group), Phys. Rev. D 45 (1992).

[26] C. Peterson *et al.*, Phys. Rev. D 27 (1983) 105.

[27] J.C. Anjos *et al.* (E691 Collab.), Phys. Rev. Lett. 65 (1990) 2503.

[28] J.C. Collins, in: Proc. XXVth Rencontre de Moriond: High Energy Hadronic Interactions (Les Arcs, March 1990), ed. J. Tran Thanh Van (Editions Frontieres, Gif-sur-Yvette, 1990) p. 123.

[29] S.J. Brodsky, C. Peterson and N. Sakai, Phys. Rev. D 23 (1981) 2745.

[30] M. Burkardt and B.J. Warr, Phys. Rev. D 45 (1992) 958. J.D. Bjorken, private communication.

[31] T. Bolton, Nevis R#1501.

[32] D. Bortoletto *et al.* (CLEO Collab.), Phys. Rev. D 37 (1988) 1719.

[33] A. Bodek *et al.*, Phys. Rev. Lett. 50 (1983) 1431; 51 (1983) 534.

[34] P. Amaudruz *et al.* (NMC Collab.), Phys. Lett. B 295 (1992) 159.

[35] A.C. Benvenuti *et al.* (BCDMS Collab.), Phys. Lett. B 223 (1989) 485; B 237 (1990) 592.

[36] A. Donnachie and P.V. Landshoff, Z. Phys. C 61 (1994) 139.